Volume 1 | Number 1 | Jan 2013 | Pages 1–100

Nanoscale

www.rsc.org/nanoscale

ROYAL SOCIETY OF CHEMISTRY

ROYAL SOCIETY OF CHEMISTRY

www.rsc.org/nanoscale

Journal Name

ARTICLE

Rational Fabrication of Gold-coated AFM TERS tip by Pulsed Electrodeposition†

Li-Kun Yang,‡ Teng-Xiang Huang,‡ Zhi-Cong Zeng, Mao-Hua Li, Xiang Wang, Fang-Zu Yang,* and Bin Ren*

Reproducible fabrication of sharp gold- or silver-coated tips becomes the bottleneck issue of tip-enhanced Raman spectroscopy, especially for the atom force microscopy (AFM)-based TERS. Herein, we developed a novel method based on pulsed electrodeposition to coat gold thin layer over atomic force microscopy (AFM) tips to produce plasmonic TERS tips with a high reproducibility. We systematically investigated the influence of the deposition potential and step time on the surface roughness and sharpness. This method allows the rational control of the radii of gold-coated TERS tips from a few to hundreds nanometers, which allows us to systematically study the dependence of the TERS enhancement on the radius of the gold-coated AFM tip. The maximum TERS enhancement was achieved for the tip radius in the range of 60~75 nm in the gap mode. The coated gold layer has a strong adhesion with the silicon tip surface, which is highly stable in water, showing the great potential for the application in the aqueous environment.

Introduction

Tip-enhanced Raman spectroscopy (TERS) is a combination of scanning probe microscopy (SPM) and Raman spectroscopy, providing not only a high detection sensitivity down to single-molecule level but also a very high spatial resolution down to sub-nanometer[1]. To date, TERS has shown wide application in fields, such as surface science,[1-4] nanomaterials,[5-8] biological systems,[9-13] catalysis,[4, 14-16] and molecular electronics.[17] It is recognized that the huge enhancement and high spatial resolution is a combined contribution of the localized surface plasmons and the lightning-rod effect, which are further determined by the tip configuration and tip material.[18, 19]

Scanning tunneling microscope (STM) and atomic force microscope (AFM) are commonly employed to build TERS systems, which determine the two types of TERS tips: STM TERS tip and AFM TERS tip. The most important way to fabricate the STM TERS tip with a high success rate is the electrochemical etching method. High quality gold[20, 21] and silver[22] tips have been obtained by this method. However, STM-based TERS can only be applied to conductive samples, which significantly restricts its application. Conversely, AFM-based TERS system is a promising tool for characterizing a wide range of materials and studying biological systems. The most prevalent method for preparing the AFM TERS tip is to use the vacuum evaporation method to deposit gold or silver onto the surface of commercial silicon tips. This method requires a very strict control over all the deposition parameters.

As a result, tips with different topography have been obtained using the same parameter in different groups or even different operators in a same group.[23-26] Other methods, such as galvanic reaction[27] and silver mirror reaction,[28] are not able to prepare the AFM TERS tip with a good reproducibility. Considerable efforts have also been devoted to producing the non-standard tips by using methods like the focused ion beam (FIB) and etc.[29-32] Unfortunately, these techniques are expensive and are not affordable by most TERS users. Up to now, fabrication of reliable AFM TERS tips is still one of the bottle necks of AFM TERS technique. It is highly desirable to develop a cost-effective method for fabricating AFM-TERS tip with a high reproducibility and efficiency.

Electrodeposition is a widely employed technique in surface finishing, anti-corrosion, and nanoscale feature fabrication for chip interconnects, microelectromechanical systems (MEMS), microelectronic packaging, and many other microelectronic and micromechanical components.[33-39] The thickness of the deposited layer can be precisely controlled from a few angstroms to several millimeters by controlling the deposition current, potential or time. Several methods have been developed to obtain the uniform coating, such as direct current, direct potential, and pulsed electrodeposition. Among them, pulsed electrodeposition has been widely used for fabrication of nanostructures over nanopore arrays with high aspect ratios to produce ultrahigh dense nanowire arrays with a diameter of 10~130 nm and length of 1~2 μm.[40-43] It has also been commonly used for the electrodeposition of thin metallic films.

In the case of AFM tips, they are of a three-dimensional structure with a very sharp apex. The gold ions in the bath will diffuse three-dimensionally to the silicon tip apex and two-dimensionally to the silicon tip body. Therefore, gold will be deposited much faster on the tip apex than that on the tip body when using a constant potential deposition method. However, by using the pulsed electrodeposition method, the slow diffusion-driven transport in the tip body will be compensated so that a uniform gold layer might be achieved. In this work, we adopted the pulsed electrodeposition method to fabricate smooth gold-coated AFM tips to be used as TERS tips. We systematically investigated the effect of the deposition potential and time on the tip morphology and radius. The optimized parameters for achieving the maximum enhancement were obtained. The unique advantage of such an electrodeposition method is the strong adhesion of the gold layer on the silicon tip surface. As a result, the gold-coated AFM tips are highly stable upon immersion in water, showing a great potential for the tip-enhanced Raman study in the aqueous environment, including electrochemistry.

Experimental section

The electrodeposition bath consists of 2 g/l of potassium dicyanoaurate ($KAu(CN)_2$), 80 g/l of potassium citrate ($K_3C_6H_5O_7 \cdot H_2O$), 40 g/l of citric acid ($C_6H_8O_7 \cdot H_2O$), 85 g/l of sodium phosphate ($Na_3PO_4 \cdot H_2O$), and a small amount of proprietary additive.[44] The pH of the bath was adjusted to 4.5 with citric acid and NaOH. All the chemicals mentioned above were of analytic reagent grade and used as received without further purification. Millipore ultrapure water (18 MΩ) was used throughout the experiments.

The electrochemical setup for electrodeposition of the tip was based on the conventional three electrodes configuration, as shown in the inset of Figure 1a. The working electrode was a silicon AFM tip (VIT_P, NT-MDT) with a tip radius (R_{tip}) of 7~10 nm and resistivity (ρ) of 0.01~0.025 $\Omega \cdot$cm. A platinum foil with an area 1 cm^2 was used as the counter electrode. The reference electrode was a Ag/AgCl reference electrode with a potential of -0.197 V vs. standard hydrogen electrode. All the potentials given in this work were relative to this reference electrode. The distance between the working and reference electrodes was about 1 cm. All the electrochemical experiments were controlled by an Autolab PGSTAT30 potentiostat/galvanostat. The temperatures of the bath were controlled at 50 °C for electrodeposition.

The shape of tip was characterized using scanning electron microscope (SEM) (Hitachi, S-4800) operated at an accelerating voltage of 15 kV with a working distance of 8~9 mm.

An upright Raman microscope (NTEGRA Spectra, NT-MDT) was employed for the TERS measurement (Figure 1b). The system is equipped with an upright confocal laser microscope, an atomic force microscope (AFM), and a white-light video microscope for rough observation/alignment of the sample and tip. The TERS experiments were performed in the

tapping mode. Optical measurements in air were performed using a 100× long working-distance objective with a numerical aperture (NA) of 0.7 for both excitation and collection of the backscattered light from the sample. The p-polarized He-Ne beam (632.8 nm) was used for TERS investigations.

A high quality Au(111) single-crystal surface was prepared by flame-annealing following the Clavilier method,[45] and then electrochemically polished to obtain an atomically flat surface. Malachite green isothiocyanate (MGITC) was used as a probe molecule. Monolayer adsorption of the MGITC was accomplished by immersing freshly flame-annealed Au(111) single crystal in a 6 μM MGITC ethanolic solution for 3 h. Then the electrode was rinsed with copious amounts of ethanol to remove physisorbed multilayer species. Finally, the Au(111) was dried under a N_2 gas flow.

For TERS measurements in liquid, the setup is the same as that used in air system except for a 100× water immersion lens with an NA of 1.0. For this purpose, (4'-(pyridin-4-yl)-biphenyl-4-yl)methanethiol (PBT),[46] a molecule that can bind strongly to the Au surface, was used as the probe molecule. The monolayer of adsorbed PBT was prepared by immersion of freshly flame-annealed Au(111) single crystal in 20 μM PBT ethanolic solution for 0.5 h. Unbound or weakly bound molecules were rinsed off with copious amounts of ethanol. Subsequently, the Au(111) was dried under a N_2 gas flow.
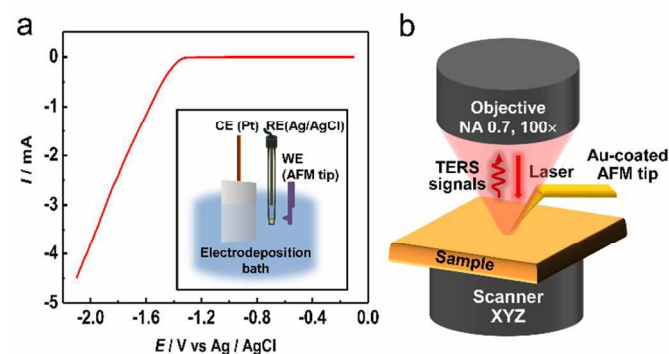

Figure 1. (a) Linear sweep voltammogram of a Si tip in the Au electrodeposition bath. Scan rate, 50 mV/s. (b) Experimental setup of the tip-enhanced Raman spectroscopy.

Results and discussion

3.1 Tip preparation

Pulsed electrodeposition was used to coat the silicon AFM tips with Au. Before electrodeposition, the silicon tips were etched in a HF buffer solution for 2 min to remove the native oxide layer. To obtain a smooth Au film on the fresh silicon surface, the composition of the bath is crucial and has been optimized in our previous work.[44] Figure 1a shows the linear sweep voltammogram of a silicon tip in the Au electrodeposition bath, which clearly shows the onset deposited potential of about 1.32 V. The current increases almost linearly with the negative scan of the potential. No diffusion-control character could be observed because of the small size of tip and a high

concentration of gold ions in the electrodeposition bath. The principle of the pulsed electrodeposition process was shown in Figure 2 and consists of two deposition pulses. The tip was first kept at the open circuit potential (E_o), then the potential was modulated to the deposition potential (E_d) for milliseconds to deposit gold. Then the potential was returned to E_o to terminate the deposition process and recover the concentration of gold ion in the interface. The deposition pulsed was repeated once. The step times (t_s) in pulsed electrodeposition process were controlled from 5 ms to 150 ms to control the thickness of the gold layers. As the tip has a three-dimensional structure and the electric field at the tip apex is high, subconformal coating will happen as a result of the high current at the tip apex. Therefore, the selection of an appropriate deposition potential is necessary to reduce the differences of deposition rate between the tip apex and tip bulk. The E_d was chosen in the overpotential range between -1.65~-1.95 V, which can not only reduce subconformal coating, but also allow the formation of large amounts of nucleation sites, which is essential to obtain a uniform Au layer. The E_o (-0.2 V) was applied so that no net electrochemical reaction occurred and the concentration the gold ion at the tip surface could be recovered before the subsequent deposition pulse. Such a potential control improves the homogeneity of the deposition and prevents the excessive hydrogen evolution on the silicon surface.
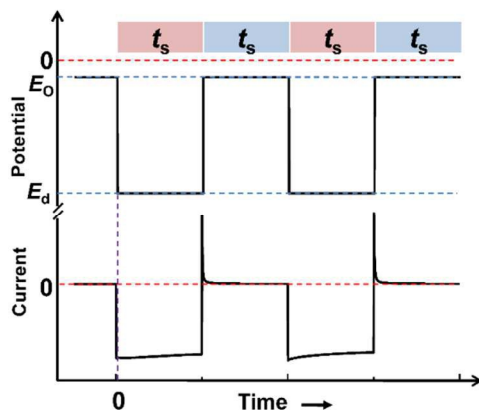

Figure 2. Schematic diagram of pulsed electrodeposition parameters to prepare Au-coated tips: the applied potential waveform (upper panel) and the detected current response (lower panel) with time. E_o: the open circuit potential, E_d: the deposition potential, t_s: the pulse width, usually in the milliseconds. Only two deposition pulse is necessary in this work.

From the linear sweep voltammogram, it is clear that the deposition potential will have a sharp influence the deposition rate, which might then result in different morphologies of the Au-coated tips. We studied four deposition potentials, -1.65, -1.75, -1.85, and -1.95 V, while keeping all other parameters the same (i.e., E_o = -0.2 V, t_s = 50 ms). The Au-coated tips were then examined by SEM to determine the surface roughness and curvature radius of the tip, and the SEM images of them were

shown in Figure 3. It can be seen clearly from Figure 3a that the tip has a small curvature radius (about 43 nm), but the coated film shows a relatively high surface roughness at the deposition potential of -1.65 V. The surface of these two tips obtained at the potentials of -1.75 and -1.85 V presents a fairly smooth structure (Figure 3b and 3c). The curvature radius is about 48 and 51 nm, respectively. Furthermore, the tip prepared at -1.85 V has a more regular tip apex. When the deposition potential was moved to -1.95 V, the tip apex becomes blunt with a curvature about 83 nm. In addition, the coating is scorched and rough due to the high overpotential. It can be concluded that silicon tips can be controllably coated with nanometer Au layer by tuning the deposition potential via the pulsed electrodeposition method. On considering both the curvature radius and the surface roughness, we chose -1.85 V as the optimal deposition potential.
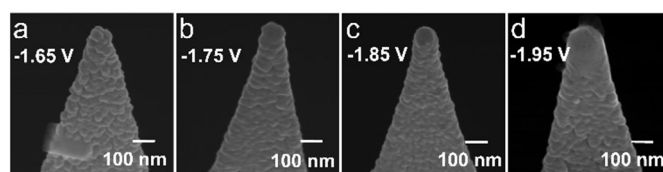

Figure 3. SEM images of Au-coated tips prepared at different deposition potentials (E_d): (a) -1.65 V, (b) -1.75 V, (c) -1.85 V, (d) -1.95 V. The other parameters were the same: E_o = -0.2 V, t_s = 50 ms.

The deposition time will also influence the amount of Au coated on the tip at a same deposition potential. We changed the step times to investigate the effect of deposition time on the curvature radius of the Au-coated AFM tip. We used the deposition potential E_d = -1.85 V according to the above study. Figure 4 shows the SEM images of four tips prepared with different step times, t_s = 20, 35, 50, and 65 ms. As shown in Figure 4a, a sharp tip with tip radius (R_{tip}) of 33 nm can be produced with the step time of 20 ms. With the increase of the step time, the radii of the tips were increased to 40, 51, and 66 nm (Figure 4b, 4c and 4d). Thus, Au-coated AFM tips with different sizes can be obtained by controlling the step times (t_s).
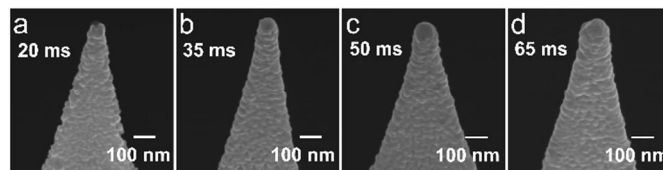

Figure 4. SEM images of Au-coated tips prepared at different step time (a) 20 ms, (b) 35 ms, (c) 50 ms, (d) 65 ms. The deposition and recovery potentials were -1.85 and -0.2 V, respectively.

Therefore, by controlling the deposition potential and deposition time, we have successfully fabricated the Au-coated AFM tips with different tip radii and roughness by the pulsed electrodeposition. Indeed, it is a great challenge to control the

entire tip with exactly the same feature at the nanometer scale. However, we should point out that the electrodeposition method shows unique advantage over vacuum based method in the following aspects: (1) in vacuum method, the pressure in the chamber significantly influence the morphology of the tip, while in the aqueous solution, the concentration of the gold ion can be precisely controlled; (2) the substrate temperature is not commonly controlled in vacuum deposition method. Therefore, depending on the chamber size and deposition parameter, the substrate temperature may vary, which will lead to different surface structure of the obtained tips. Whereas the deposition temperature can be precisely controlled by controlling the bath temperature in electrodeposition. (3) The silicon surface can be chemically cleaned to have a same chemical property before electrodeposition. All the features ensure the high reproducibility of the tips prepared by the pulsed electrodeposition method. It should be noted that we listed only the most representative SEM images obtained for the specific parameter. In the next part, we will test the TERS activity of 22 tips, and a trend can be obtained, which further demonstrates a high reproducibility of the method.

3.2 TERS study

SEM images alone cannot be used to determine whether a tip is TERS active or not. The most direct way is to check the TERS signal of our tips with different thickness of the coating layer. In fact, there have been a number of reports on the influence of tip apex and tip-sample separation on the tip-enhanced Raman signal.[47-50] With a same instrumental configuration, the radius of the tip apex was found to be the dominant factor determining the field enhancement. Whereas, the optimal tip radius depends on the substrate beneath the tip apex.[19, 51-54] Especially, when a Au or Ag substrate is used, it automatically forms a plasmon-coupled gap configuration with the tip. Theoretical calculations revealed that the maximum TERS enhancement can be achieved when the tip radius is in the range of 50~100 nm.[19, 52, 53] Unfortunately, up to now there is still no systematical experimental report about the influence of tip radius on the tip-enhanced Raman signal, because the low reproducibility in controlling the coating layer of the tip apex.

To test the TERS activity of the above Au-coated AFM tips, we chose a Au (111) single crystal as the substrate. In this way, the Au tip and Au substrate form a coupled system that can produce strong signal and enables us to perform detailed and reliable analysis of the tip quality. Before the TERS measurement, we measured the background signal of the as-prepared Au-coated tip by acquiring the TERS spectra of the tip on a clean Au(111) surface. As shown in Figure 5a, we can only observe one peak at ~ 520 cm^{-1} attributed to the first order lattice phonon vibration of the Si tip. Hence, the Au-coated AFM tip fabricated by pulsed electrodeposition method is suitable for TERS study without giving interfering background signals for most organic species.

We then chose MGITC as the probe molecule. When the tip is far away from the Au(111) surface, i.e., without TERS enhancement, the MGITC monolayer over Au(111) can already

give a weak but detectable signal, see Figure 5b bottom spectrum. The signal provides a convenience reference signal for calculation of the enhancement factor of the tip. In contrast, when the tip approaches the Au(111) surface, very strong TERS signal can be obtained. We tested the TERS signal of 22 tips with different coating thickness. The most representative TERS spectrum under the approached condition was shown as the top spectrum in Figure 5b.

The absolute signal intensity is not necessarily a good indicator of the high field enhancement, because for tips with different radii, the number of molecules detected may be different. In fact, the contrast factor (C) and TERS enhancement factor (EF_{TERS}) are the two accepted important parameters to reflect the electric field enhancement of the tip.[29] By definition, the contrast factor(C) can be obtained by:

$$C = \frac{S_{NF}}{S_{FF}} \qquad (1)$$

where S_{NF} is the TERS signal when the tip is approached, and S_{FF} is the background signal when the tip is retracted. Contrast factor is of more practical relevance, because it is a direct measure for the signal increase in the presence of the tip, and determines the imaging contrast in TERS. However, in order to compare with the theoretical calculation, it is better to calculate the TERS enhancement factor to consider the difference in the sampling area in the far-filed and near-field configuration:[29]

$$EF_{TERS} = \frac{S_{NF} - S_{FF}}{S_{FF}} \times \frac{A_{FF}}{A_{NF}} = (\frac{S_{NF}}{S_{FF}} - 1) \times \frac{R_{laser}^2}{R_{tip}^2} \qquad (2)$$

where the A_{FF} and A_{NF} are the sampling areas in far-field and near-field configurations, respectively. R_{laser} is the radius of the laser focus and R_{tip} is the radius of the tip apex.
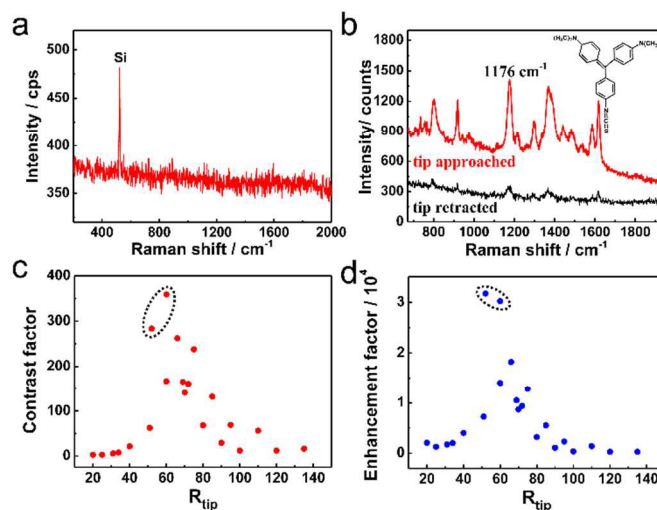

Figure 5. TERS characterization of the Au-coated AFM tip. (a) TERS spectra of the tip approach to a clean Au (111) single-crystal (0.5 mW, 1 s). (b) Raman spectra of MGITC monolayer when the tip was approached (upper spectrum, 0.1 mW, 3 s) and retracted (lower spectrum, 0.5 mW, 10 s). (c) The dependence of the contrast factor on the tip radius, using the intensity of the peak at 1176 cm^{-1}. (d) The dependence of the

TERS enhancement factor on the tip radius, using the intensity of the peak at 1176 cm^{-1}.

Figure 5c and 5d show the dependence of the contrast factor and the TERS enhancement factor on the tip radius, respectively. These two factors increase sharply with the increase of the tip radius from 20 nm to 65 nm. Further increase of the tip radius will lead to the decrease of the two factors. The data inside the circle might be the singular points, which may be a result of the surface nanostructure on the tip apex. But the overall trend is impressive, because it presents such a strong dependence of the enhancement with the tip radius. The maximum contrast factor is about 260, implying that the detected Raman signals was 260 times higher than that of the normal Raman signal of MGITC due to the strong coupling between the Au-coated tip and the Au(111) surface. Furthermore, the maximum TERS enhancement factor can be achieved for the tip radius of 60~75 nm, which is in good agreement with the theoretical predictions.[52] However, it should be noted that the maximum TERS enhancement factor is about 4 orders of magnitude lower than that predicted in theory (10^9). Such a difference is reasonable due to the following three facts: (1) In the tapping mode AFM, the tip is intermittently approaching the surface, and the time for the tip to be in the effective coupling distance is much shorter than the real acquisition time of a TERS spectrum. (2) The theoretical calculation value is the maximum value instead of the average over the sampling area. (3) Under the approaching condition, the tip will block a certain amount of excitation light and the signal for the top illumination setup. On considering these facts, our experimental data agree well with the theoretical prediction.

The good trend in Figure 5c and 5d reflects that the tip produced by pulsed electrodeposition method is highly reproducible. Figure 6 shows the SEM images and TERS spectra MGITC spectra of two tips prepared with the same parameter, but in different batches. It can be clearly seen that these two tips have similar radii and TERS enhancement. This result further convincingly demonstrates that the as-developed method has a high reproducibility.
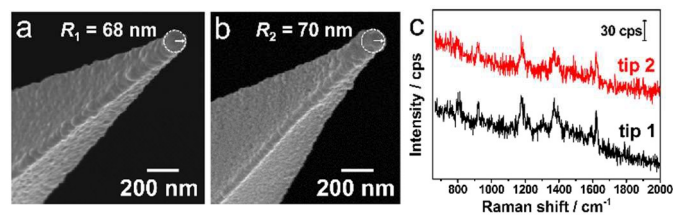

Figure 6. SEM images (a and b) and TERS spectra (c) of MGITC monolayer of two tips prepared with the same parameter in different batches. Tip preparation: E_d = -1.85 V, t_s = 70 ms. Laser power for TERS measurement: 11 µW.

3.3 Performing TERS in liquid

There is an increasing request on performing TERS in liquid systems. However, most of the previous AFM based TERS tips were prepared by the vacuum deposition methods. Due to the weak adhesion of the metal layer with the tip substrate, the metal layer will usually peel off upon soaking into liquids.[55] We first checked the stability of Au-coated AFM tip in a liquid environment before performing TERS in liquid. Figure 7a and 7b show the SEM images of Au-coated AFM tip before and after soaking in water for 3 h, and we managed to take the images of a same tip at the same angle and direction. Impressively, no peel-off of the coating layer can be observed, indicating a strong adhesion between the coated layer with the substrate. In the electrodeposition process, the gold ion obtained electron from the electrode and deposited on ultraclean surface. By this way, there is a high bonding strength between Au layer with the substrate. Furthermore, since the Au coating layer fabricated by electrodeposition method is a continuous film, it has a better resistance to the soaking of the electrolyte into the gap between the Au layer and the substrate. Looking into the detailed morphology of the tip, we can find that most of the grains and nanostructures still retain. We only observe slight smooth off the sharp feature probably due to the ripening of the sharp feature.

We used the tip for the preliminary TERS measurement in water. As the interaction of MGITC with the Au surface is not strong enough to avoid desorption in water, it may be desorbed from the surface and re-adsorbed on the tip to complicate the result. Therefore, we used another molecule, PBT, with thiol group as a probe molecule. PBT can form a self-assemble layer via strong interaction of the thiol group with gold. However, PBT is not in resonance with 632.8 nm wavelength, and no observable Raman signal can be detected in the far-field spectrum on Au(111) surface in the absence of the tip, see lower spectrum in Figure 7c. However, when the tip approaches the sample, the characteristic Raman peaks at 1605 and 1282 cm^{-1} of PBT appear, see upper spectrum in Figure 7c.[56] The above result clearly demonstrates that Au-coated tip prepared by pulsed electrodeposition can be used for TERS study in water.
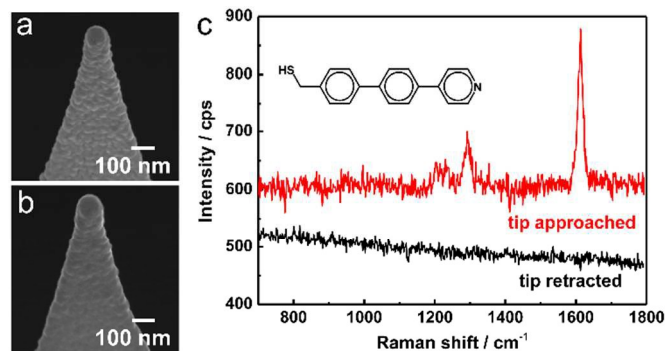

Figure 7. SEM images of Au-coated AFM tips (a) before and (b) after soaking in water for 3 h, and TERS measurements of a SAM of PBT on Au(111) surface collected in water. Laser power: 0.32 mW. Acquisition time: 1 s.

Conclusions

In summary, we have developed a pulsed electrodeposition method to conveniently coat over commercially available AFM tips with a gold layer, and successfully fabricated TERS tips with a high reproducibility and good enhancement. The surface morphology of the coated gold layer can be controlled by the deposition potential and the tip radius can be controlled by the deposition time. Such a pulsed electrodeposition method shows good control of the deposited layer and good reproducibility. Benefited from this feature, we have been able to reproducibly obtain a series of tips with different tip radii and systematically investigated the effect of the tip radius on the TERS enhancement. The maximum TERS enhancement can be achieved for the tip radius of 60~75 nm when the tip is coupled with Au substrate. Most importantly, the gold layer fabricated following this method are highly stable due to the strong interaction between the coating layer and the silicon tip surface. The layer is stable even after immersion in the aqueous solution, which is highly promising to be used for TERS study in the aqueous environment important to electrochemical TERS and biological studies. Furthermore, this method is cost-effective and convenient, and will be highly attractive to the TERS community.

Acknowledgements

Notes and references

State Key Laboratory of Physical Chemistry of Solid Surface, Collaborative Innovation Center of Chemistry for Energy Materials (iChEM), Key Laboratory of Analytical Sciences, Department of Chemistry, College of Chemistry and Chemical Engineering, Xiamen University, Xiamen 361005, China.

E-mail: fzyang@xmu.edu.cn ; bren@xmu.edu.cn ; Tel: +86-592-2186532.

† Electronic Supplementary Information (ESI) available. See DOI: 10.1039/b000000x/

‡ These authors contributed equally to the work.

TOC
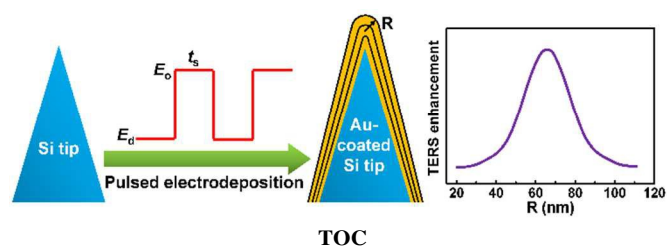
1. R. Zhang, Y. Zhang, Z. C. Dong, S. Jiang, C. Zhang, L. G. Chen, L. Zhang, Y. Liao, J. Aizpurua, Y. Luo, J. L. Yang and J. G. Hou, *Nature*, 2013, **498**, 82-86.
2. Z. L. Zhang, S. X. Sheng, H. R. Zheng, H. X. Xu and M. T. Sun, *Nanoscale*, 2014, **6**, 4903-4908.
3. Z. Liu, X. Wang, K. Dai, S. Jin, Z. C. Zeng, M. D. Zhuang, Z. L. Yang, D. Y. Wu, B. Ren and Z. Q. Tian, *J. Raman. Spectrosc.*, 2009, **40**, 1400-1406.
4. E. M. V. Lantman, T. Deckert-Gaudig, A. J. G. Mank, V. Deckert and B. M. Weckhuysen, *Nat. Nanotechnol.*, 2012, **7**, 583-586.
5. A. Hartschuh, E. J. Sánchez, X. S. Xie and L. Novotny, *Phys. Rev. Lett.*, 2003, **90**, 095503.
6. J. Stadler, T. Schmid and R. Zenobi, *Acs Nano*, 2011, **5**, 8442-8448.
7. Y. Saito, M. Motohashi, N. Hayazawa, M. Iyoki and S. Kawata, *Appl. Phys. Lett.*, 2006, **88**, 3.
8. D. Zhang, U. Heinemeyer, C. Stanciu, M. Sackrow, K. Braun, L. E. Hennemann, X. Wang, R. Scholz, F. Schreiber and A. J. Meixner, *Phys. Rev. Lett.*, 2010, **104**, 056601.
9. K. Olschewski, E. Kammer, S. Stockel, T. Bocklitz, T. Deckert-Gaudig, R. Zell, D. Cialla-May, K. Weber, V. Deckert and J. Popp, *Nanoscale*, 2015, **7**, 4545-4552.
10. K. F. Domke, D. Zhang and B. Pettinger, *J. Am. Chem. Soc.*, 2007, **129**, 6708-6709.
11. U. Neugebauer, P. Rösch, M. Schmitt, J. Popp, C. Julien, A. Rasmussen, C. Budich and V. Deckert, *ChemPhysChem*, 2006, **7**, 1428-1430.
12. E. Bailo and V. Deckert, *Angew. Chem. Int. Ed.*, 2008, **47**, 1658-1661.
13. B. R. Wood, M. Asghari-Khiavi, E. Bailo, D. McNaughton and V. Deckert, *Nano Lett.*, 2012, **12**, 1555-1560.
14. N. Kumar, B. Stephanidis, R. Zenobi, A. J. Wain and D. Roy, *Nanoscale*, 2015, **7**, 7133-7137.
15. Z. L. Zhang, L. Chen, M. T. Sun, P. P. Ruan, H. R. Zheng and H. X. Xu, *Nanoscale*, 2013, **5**, 3249-3252.
16. Z. L. Zhang, M. T. Sun, P. P. Ruan, H. R. Zheng and H. X. Xu, *Nanoscale*, 2013, **5**, 4151-4155.
17. Z. Liu, S. Y. Ding, Z. B. Chen, X. Wang, J. H. Tian, J. R. Anema, X. S. Zhou, D. Y. Wu, B. W. Mao, X. Xu, B. Ren and Z. Q. Tian, *Nat. Commun.*, 2011, **2**, 305.
18. E. Bailo and V. Deckert, *Chem. Soc. Rev.*, 2008, **37**, 921-930.
19. Z. L. Yang, J. Aizpurua and H. X. Xu, *J. Raman. Spectrosc.*, 2009, **40**, 1343-1348.
20. B. Ren, G. Picardi and B. Pettinger, *Rev. Sci. Instrum.*, 2004, **75**, 837-841.
21. X. Wang, Z. Liu, M. D. Zhuang, H. M. Zhang, Z. X. Xie, D. Y. Wu, B. Ren and Z. Q. Tian, *Appl. Phys. Lett.*, 2007, **91**, 101105.
22. W. H. Zhang, B. S. Yeo, T. Schmid and R. Zenobi, *J. Phys. Chem. C*, 2007, **111**, 1733-1738.
23. B. S. Yeo, W. H. Zhang, C. Vannier and R. Zenobi, *Appl. Spectrosc.*, 2006, **60**, 1142-1147.
24. N. Hayazawa, T. Yano and S. Kawata, *J. Raman. Spectrosc.*, 2012, **43**, 1177-1182.
25. V. Deckert, T. Deckert-Gaudig, M. Richter, R. Treffer and X. M. Lin, in *Biomedical Vibrational Spectroscopy Iv: Advances in Research and Industry*, eds. A. MahadevanJansen and W. Petrich, Spie-Int Soc Optical Engineering, Bellingham2010, vol. 7560, pp. 75600J-75600J-75610.
26. M. Asghari-Khiavi, B. R. Wood, P. Hojati-Talemi, A. Downes, D. McNaughton and A. Mechler, *J. Raman. Spectrosc.*, 2012, **43**, 173-180.
27. P. R. Brejna and P. R. Griffiths, *Appl. Spectrosc.*, 2010, **64**, 493-499.

28. Y. Saito, T. Murakami, Y. Inouye and S. Kawata, *Chem. Lett.*, 2005, **34**, 920-921.

29. J. Stadler, T. Schmid and R. Zenobi, *Nanoscale*, 2012, **4**, 1856-1870.

30. P. J. Schuck, A. Weber-Bargioni, P. D. Ashby, D. F. Ogletree, A. Schwartzberg and S. Cabrini, *Adv. Funct. Mater.*, 2013, **23**, 2539-2553.

31. M. Fleischer, A. Weber-Bargioni, M. V. P. Altoe, A. M. Schwartzberg, P. J. Schuck, S. Cabrini and D. P. Kern, *ACS Nano*, 2011, **5**, 2570-2579.

32. Y. Yang, Z. Y. Li, M. Nogami, M. Tanemura and Z. R. Huang, *RSC Advances*, 2014, **4**, 4718-4722.

33. M. P. Zach, K. H. Ng and R. M. Penner, *Science*, 2000, **290**, 2120-2123.

34. T. Thurn-Albrecht, J. Schotter, C. A. Kastle, N. Emley, T. Shibauchi, L. Krusin-Elbaum, K. Guarini, C. T. Black, M. T. Tuominen and T. P. Russell, *Science*, 2000, **290**, 2126-2129.

35. M. Datta, *Electrochim. Acta*, 2003, **48**, 2975-2985.

36. L. T. Romankiw, *Electrochim. Acta*, 1997, **42**, 2985-3005.

37. T. Osaka, *Electrochim. Acta*, 1997, **42**, 3015-3022.

38. M. Datta, R. Shenoy, C. Jahnes, P. Andricacos, J. Horkans, J. Dukovic, L. Romankiw, J. Roeder, H. Deligianni and H. Nye, *J. Electrochem. Soc.*, 1995, **142**, 3779-3785.

39. P. C. Andricacos, C. Uzoh, J. O. Dukovic, J. Horkans and H. Deligianni, *Ibm. J. Res. Dev.*, 1998, **42**, 567-574.

40. K. Nielsch, R. B. Wehrspohn, J. Barthel, J. Kirschner, S. F. Fischer, H. Kronmuller, T. Schweinbock, D. Weiss and U. Gosele, *J. Magn. Magn. Mater.*, 2002, **249**, 234-240.

41. H. Natter and R. Hempelmann, *J. Phys. Chem.*, 1996, **100**, 19525-19532.

42. G. Sauer, G. Brehm, S. Schneider, K. Nielsch, R. B. Wehrspohn, J. Choi, H. Hofmeister and U. Gosele, *J. Appl. Phys.*, 2002, **91**, 3243-3247.

43. K. Nielsch, F. Muller, A. P. Li and U. Gosele, *Adv. Mater.*, 2000, **12**, 582-586.

44. *Chinese Pat.,* CN103757675A, 2014.

45. J. Clavilier, R. Faure, G. Guinet and R. Durand, *J. Electroanal. Chem.*, 1980, **107**, 205-209.

46. B. Schupbach and A. Terfort, *Org. Biomol. Chem.*, 2010, **8**, 3552-3562.

47. S. Klein, P. Geshev, T. Witting, K. Dickmann and M. Hietschold, *Electrochemistry.*, 2003, **71**, 114-116.

48. S. Klein, T. Witting, K. Dickmann, P. Geshev and M. Hietschold, *Single Mol.*, 2002, **3**, 281-284.

49. J. T. Krug, E. J. Sanchez and X. S. Xie, *J. Chem. Phys.*, 2002, **116**, 10895-10901.

50. M. Micic, N. Klymyshyn, Y. D. Suh and H. P. Lu, *J. Phys. Chem. B*, 2003, **107**, 1574-1584.

51. W. H. Zhang, X. D. Cui and O. J. F. Martin, *J. Raman. Spectrosc.*, 2009, **40**, 1338-1342.

52. L. Y. Meng, T. X. Huang, X. Wang, S. Chen, Z. L. Yang and B. Ren, *Opt. Express*, 2015, **23**, 13804-13813.

53. C. Huber, A. Trugler, U. Hohenester, Y. Prior and W. Kautek, *Phys. Chem. Chem. Phys.*, 2014, **16**, 2289-2296.

54. A. L. Demming, F. Festy and D. Richards, *J. Chem. Phys.*, 2005, **122**.

55. T. Schmid, B. S. Yeo, G. Leong, J. Stadler and R. Zenobi, *J. Raman. Spectrosc.*, 2009, **40**, 1392-1399.

56. H. X. Lin, J. M. Li, B. J. Liu, D. Y. Liu, J. X. Liu, A. Terfort, Z. X. Xie, Z. Q. Tian and B. Ren, *Phys. Chem. Chem. Phys.*, 2013, **15**, 4130-4135.